

Chitosan-Graft-Sodium Alginate Encapsulated Vanadium Pentoxide (V_2O_5) Nanocomposite for Adsorption and Antimicrobial Studies

Bernice Y. Danu¹, Eric S. Agorku^{2*}, Francis K. Ampong¹, Johannes A.M. Awudza², Bismark Owusu², Patrick N.O. Brown³, Onoyivwe M. Ama^{4,6}, Peter O. Osifo⁴ and Suprakas S. Ray^{5,6}

¹Department of Physics, Kwame Nkrumah University of Science and Technology, PMB, Kumasi, Ghana.

²Department of Chemistry, Kwame Nkrumah University of Science and Technology, PMB, Kumasi, Ghana.

³Department of Theoretical and Applied Biology, Kwame Nkrumah University of Science and Technology, PMB, Kumasi, Ghana.

⁴Department of Chemical Engineering, Vaal University of Technology, Private Mail Bag X021, Vanderbijlpark 1900, South Africa.

⁵Department of Chemical Science, University of Johannesburg, Doornfontein, 2028, Johannesburg, South Africa.

⁶DST-CSIR National Center for Nanostructured Materials, Council for Scientific and Industrial Research, Pretoria 0001, South Africa.

*Correspondence:

Eric S. Agorku, Department of Chemistry, Kwame Nkrumah University of Science and Technology, PMB, Kumasi, Ghana.

Received: 02 December 2021; **Accepted:** 30 December 2021

Citation: Danu BY, Agorku ES, Ampong FK, et al. Chitosan-Graft-Sodium Alginate Encapsulated Vanadium Pentoxide (V_2O_5) Nanocomposite for Adsorption and Antimicrobial Studies. J Adv Mater Sci Eng. 2021; 1(1): 1-10.

ABSTRACT

A hybrid vanadium pentoxide (V_2O_5)/chitosan-graft-sodium alginate nanocomposite was synthesized via the graft co-polymerization technique. The nanocomposite was characterized by X-ray diffraction analysis, Fourier transform infra-red spectroscopy, scanning electron microscopy and transmission electron spectroscopy. Batch studies was employed for the adsorption of model methyl violet onto V_2O_5 /chitosan-graft-sodium alginate from aqueous solution. The adsorption best suited the Langmuir isotherm and pseudo-second order kinetic model. The positive value of the change in enthalpy, ΔH° (6.62 kJ/mol.) established an endothermic process. The negative values of the free Gibbs energy, ΔG° (-4.19 to -4.87 kJ/mol.K) within the range of temperatures of 300 K to 318 K, indicated that the adsorption process was thermodynamically favourable and spontaneous. The value of the change in entropy, ΔS° (0.035 kJ/mol) revealed a randomness in the adsorption process. These outcomes show a potential use of V_2O_5 /chitosan-graft-sodium alginate composite for the removal of organic dyes from polluted water.

Keywords

Adsorption, Chitosan, Sodium alginate, Graft copolymerization, V_2O_5 .

Introduction

Safe water for human consumption and other uses is becoming increasingly scarce in recent times. This is due to increasing demand of water resources and contamination by natural and

anthropogenic means [1]. Industries such as textile, dyeing, paint and leather tanning are major contributors of the release of wastewater [1,2]. The wastewater released after the dyeing and finishing processes from textile plants is considered the most contaminating of all the industrial sources, taking into account the magnitude and composition of the released effluents [3-6]. As demand for textile products is rising, there is a proportionate increase in effluent output as well. The use of synthetic dyes in the

manufacture of textile products has contributed greatly in recent times to the source of water contamination. The effects of these pollutants, even if they are smaller than < 1 mg/L in water, can seriously affect the consistency and clarity of most water bodies [7]. Some of these dyes are mutagenic and highly toxic, reduce light penetration and subsequent photosynthetic activity. This affects the oxygen supply necessary for aquatic life survival [8,9]. Dyes are engineered to resist biodegradation in such a way that they survive for a considerably long time in the climate [10].

Several wastewater remediation methods such as coagulation, chemical oxidation, membrane separation and adsorption have been employed over the years to remedy the wastewater contamination [11]. However, among these methods, adsorption presents itself as advantageous due to it being effective, economical and ease of use.

Polymeric nanoparticles have generated considerable attention due of their distinctive properties and ease of surface modification [12,13]. Incorporation of nanoparticles within the polymer matrix enhances the surface area and improves the binding capabilities [14].

Vanadium pentoxide (V_2O_5) is a useful ceramic that has spurred massive investigation in the use of optical switching devices, catalysis, sensors, etc. [15–17]. Due to its low isoelectric point (1–1.5) in aqueous solution, its surface becomes negatively charged and can be used to attract cationic dyes [18].

Alginate is a an environmentally friendly and biocompatible polymer having numerous applications [19,20]. It is a naturally polyanionic polysaccharide obtained from brown sea weed and comprises of alternating units of 1,4- linked β -D-mannuronic and α -L-guluronic acid [21]. However, alginate has the tendency to form films whose water resistance is deficient owing to the presence of hydroxyl and carboxylic groups [21]. To improve the properties of alginate, it is crosslinked with metal ions such Ca^{2+} or polyamines like chitosan which can network with it to produce insoluble polymers [21].

Chitosan is a cationic polysaccharide with biodegradability, biocompatibility and bioabsorbable properties [22]. It is derived from the deacetylation of chitin [23]. Chitosan and alginate have been reported as excellent biomaterials for numerous applications [1,21,24–26]. Literature has shown that no work has been done on the synthesis of V_2O_5 impregnated chitosan-graft- sodium alginate nanocomposite for dye adsorption.

Herein, this work reports a novel V_2O_5 / chitosan graft sodium alginate nanocomposite for the adsorption of model dye, methyl violet, from water and antimicrobial studies. The effects of adsorption parameters were investigated and analysed by different adsorption isotherms. Thermodynamic studies as well as antimicrobial studies were also conducted.

Materials and Methods

Materials

All chemicals utilized were of analytical grade and used without further treatment. Sodium alginate (SA), chitosan (Ch), acetic acid,

oxalic acid, glycerol, methyl violet (MV) and vanadium pentoxide (V_2O_5) were procured from Sigma-Aldrich, Germany.

V_2O_5 nanoparticle (NP) synthesis

V_2O_5 (3.6 g) powder was added to 20 ml deionized water with constant stirring and 2 ml of glycerol was added whilst on a magnetic hot plate stirrer. Oxalic acid (7.6 g) was then added and the resulting mixture heated at $80^\circ C$ for 3 hours. The mixture was filtered, washed with deionized water and dried at $100^\circ C$ overnight and further heated at $200^\circ C$ for 5 h in an electric oven. The dried precipitate was ground and stored for further use.

Preparation of V_2O_5 /chitosan-g-sodium alginate (V_2O_5 /Ch-g-SA) nanocomposite

One (1) ml of (1% v/v) acetic acid was added to 100 ml volumetric flask and topped to the mark with deionized water. This solution was added to chitosan (1 g) under continuous stirring. V_2O_5 (0.5 g) nanoparticle was added to the solution and stirred for an additional 30 minutes. Sodium alginate (1 g) was mixed with 100 ml of deionized water and stirred till it dissolved. The sodium alginate solution was then added dropwise to the chitosan- V_2O_5 mixture until a precipitate was formed. The resulting mixture was stirred for 30 minutes, sonicated and washed with deionized water to remove homopolymers. The resulting precipitate formed was then dried at $80^\circ C$ in a hot air oven and pulverized for subsequent use.

Characterization

V_2O_5 NP and V_2O_5 /Ch-g-SA nanocomposite were characterised using various analytical techniques such as fourier transform infrared spectroscopy (FTIR), x-ray powder diffraction (XRD), scanning electron microscopy (SEM), transmission electron microscopy (TEM) and ultraviolet-visible (UV-Vis) spectroscopy.

Equilibrium Adsorption

The experiments were carried out at room temperature (300 ± 1 K) except for the analysis of the impact of temperature studies. Appropriate mass of V_2O_5 /Ch-g-SA nanocomposite was added to 50 ml of methyl violet (MV) solutions and shaken on a mechanical shaker at 150 rpm. Certain quantities of the dye solution (10 ml) were taken for each sample after a predetermined time. The residual MV concentration in aqueous solution was measured using a Shimadzu (UVmini-1240) UV-Visible spectrophotometer at an absorbance of 583.5 nm. The following equations were employed to determine the amount of residual dye:

$$R.E (\%) = \frac{C_0 - C_e}{C_0} \times 100$$

and

$$Q_e (mg/g) = \frac{C_0 - C_e}{M} \times V$$

where C_0 is the initial MV concentration (mg/L), C_e is the equilibrium concentration (mg/L), M is the mass of the adsorbent (g) and V is the volume of MV (L).

The impact of varying mass of V_2O_5 /Ch-g-SA was conducted by varying the mass between 0.05 g and 0.30 g using 50 ml of 100 mg/L of MV solution. The contact time impact on MV adsorption

was investigated using 0.05 g/50 ml of 50 mg/L MV solution. The influence of initial MV concentration was done within a range of 60 to 100 mg/L using 0.05 g adsorbent. The effect of pH was studied by varying pH of MV solution between 2 and 10. The impact of temperature was examined between 300 and 318 K using a MaxQ 8000 incubator shaker with 0.05 g/50 ml solution.

Adsorption Isotherms

The data obtained was fitted to the Freundlich, Langmuir and Dubinin-Radushkevich (D-R) adsorption isotherm models.

Langmuir isotherm model assumes a homogenous surface adsorption [27]. The linear form is:

$$\frac{C_e}{q_e} = \frac{1}{q_m} C_e + \frac{1}{q_m K_L} \quad (3)$$

where C_e is the residual dye concentration at equilibrium (mg/L), q_e is the amount of MV removed at equilibrium per unit mass (mg/g), q_m is the monolayer adsorption capacity of the adsorbent and K_L is the Langmuir constant (L/mg).

The Freundlich isotherm assumes a multilayer adsorption on a heterogeneous surface [28]. The linear equation is:

$$\log q_e = \frac{1}{n} \log C_e + \log K_F \quad (4)$$

where q_e is the quantity of dye adsorbed at equilibrium per unit mass (mg/g), C_e is the residual concentration at equilibrium (mg/L), K_F is the adsorbent capacity (mg/g)(L/mg) and $1/n$ is the heterogeneity factor. A linear plot of $\log q_e$ against $\log C_e$ determines the value of $1/n$ and K_F .

Dubinin-Radushkevich (D-R) isotherm is used to ascertain the mean free energy and nature of adsorption as to whether it is physical or chemical in nature [28]. The linear form is:

$$\ln q_e = \ln q_{DR} - \beta \varepsilon^2 \quad (5)$$

where q_{DR} is the D-R maximum monolayer adsorption capacity (mg/g), β is the activity coefficient (mol^2/J^2) related to the mean adsorption energy and ε can be estimated using the relation:

$$\varepsilon = RT \ln \left(1 + \frac{1}{C_e} \right) \quad (6)$$

where R is the molar gas constant (8.314 J/mol/K), T is the temperature (K) and C_e is the residual concentration of the adsorbate at equilibrium (mg/L). The mean free energy E , can be determined using:

$$E = \frac{1}{\sqrt{2\beta}} \quad (7)$$

B and q_{DR} values can be obtained from a plot of $\ln q_e$ against ε^2 .

Adsorption Kinetics

The pseudo-first order and pseudo-second order kinetics were used in this study. The pseudo-first order kinetic model is applicable at the initial stage of adsorption when the uptake rate is relatively fast [29]. The linear equation is:

$$\log(q_e - q_t) = \log q_e - k_1 t \quad (8)$$

where q_t and q_e are the amount of dye uptake at time t and equilibrium respectively (mg/g), k_1 is the pseudo-first order constant.

The pseudo-second order kinetic model is applicable over the entire adsorption process [29,30]. The linear equation is:

$$\frac{t}{q_t} = \frac{1}{k_2 q_e} + \frac{1}{q_e} t \quad (9)$$

where q_e , q_e and t are defined earlier, k_2 is the pseudo-second order constant.

Adsorption Thermodynamics

Change in enthalpy (ΔH°), change in Gibbs free energy (ΔG°) and change in entropy (ΔS°) were calculated from the following relationship:

$$\Delta G^\circ = \Delta H^\circ - T \Delta S \quad (10)$$

$$\Delta G^\circ = -RT \ln K_d \quad (11)$$

$$\ln K_d = q_e / C_e \quad (12)$$

$$\ln K_d = \frac{\Delta S^\circ}{R} - \frac{\Delta H^\circ}{RT} \quad (13)$$

where R is the molar gas constant (8.314 J/mol/K), T is the temperature (K), q_e is the amount of MV adsorbed at equilibrium (mg/g) and C_e is the amount of MV remaining in solution at equilibrium (mg/L). Equation (11) can be used to compute the values of ΔG° at various temperatures. ΔS° and ΔH° can be estimated from a plot of $\ln K_d$ against $1/T$.

Antimicrobial studies

Nutrient agar plates were prepared to determine the susceptibility of cultured microbes (*Escherichia coli*, *Bacillus megaterium* and *Staphylococcus aureus*) to both V_2O_5 NP and V_2O_5 /Ch-g-SA nanocomposite. Three tubes of 5 ml microbial suspension were prepared from the microbes grown in the nutrient broth. Wells were created on the nutrient agar plates and filled with 0.05 g of both the NP and V_2O_5 /Ch-g-SA nanocomposite. The plates were then incubated for 24 hours at 37°C. The diameter of the inhibition by both samples were recorded and the averages taken.

Results and discussion

FTIR Studies

The FTIR study was carried out in order to establish the formation of vanadium pentoxide nanoparticles (V_2O_5) and the impregnation of V_2O_5 into the graft copolymer. The IR bands of V_2O_5 nanoparticle (Figure 1b), show a broad band ranging from 3600 to 2000 cm^{-1} which may be attributed to vibrations from absorbed water molecules and hydroxyl groups. The peak at 1123 cm^{-1} was attributed to V=O stretching vibrations [31] and V-O bonds were attributed to peaks < 1000 cm^{-1} [32].

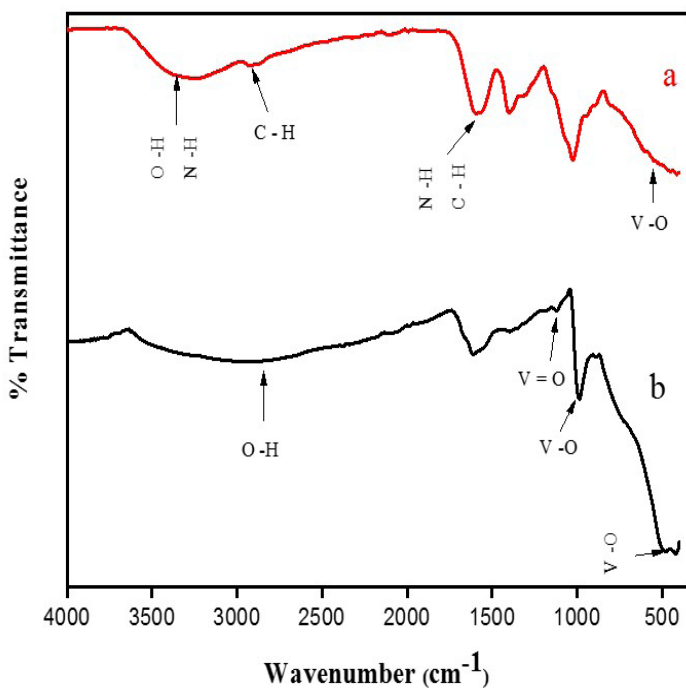


Figure 1: FTIR spectra of V_2O_5 /Ch-g-SA nanocomposite (a) and vanadium pentoxide (V_2O_5) nanoparticle (b).

In the IR spectrum of V_2O_5 /Ch-g-SA nanocomposite (Figure 1a), the peak observed at 3246 cm^{-1} suggested stretching vibration from O-H and N-H bonds. [25]. At 2880 cm^{-1} , a weak peak observed may be due to C-H stretching whereas 1596 cm^{-1} corresponds to N-H bending and C-N stretching [26,33]. Also, peaks situated at 1401 cm^{-1} and 1025.45 cm^{-1} were assigned to carboxylate group of alginates associated with chitosan [33]. Peaks ranging from 1500 to 400 cm^{-1} indicate the presence of V-O bonds hence peaks at 1123 cm^{-1} and 989 cm^{-1} and the shift in V-O peak position show that V_2O_5 nanoparticle was embedded in the polymer matrix of the chitosan-g-sodium alginate.

X-Ray diffraction analyses

The XRD patterns of V_2O_5 nanoparticles and V_2O_5 /Ch-g-SA nanocomposite are shown in Figure 2. The peaks from the V_2O_5 diffractogram (Figure 2a) at $2\theta=15.22^\circ$, 20.22° , 26.28° , 30.83° and 50.26° corresponds to 200, 001, 110, 400, 601 planes of crystalline form of an orthorhombic system (JCPDS 9-387) [34,35]. The sharp peaks observed in the XRD patterns indicate the crystallinity of the sample. However, the XRD pattern of the V_2O_5 /Ch-g-SA nanocomposite showed the amorphous nature of the composite (Figure 2b) which is mainly from the graft biopolymers. This may be ascribed to the disruption in the close packing that arises from the grafting of alginate with chitosan [21,36-38].

Using the Scherrer's equation, the crystalline size of the samples were calculated:

$$D = \frac{0.9\lambda}{\beta \cos\theta} \quad (14)$$

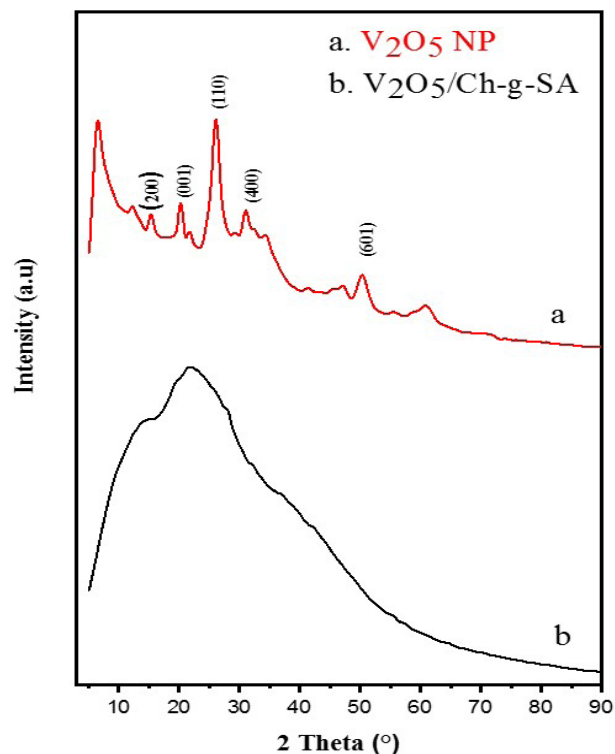


Figure 2: XRD patterns of V_2O_5 nanoparticles (a) and V_2O_5 /Ch-g-SA nanocomposite (b).

where the wavelength of the X-ray (nm) is given by λ , β is the full width at half maximum (FWHM) of the diffraction peak (radian), the angle of diffraction at the maximum intensity is given by θ and D is the average crystalline size of the sample under investigation. The average crystalline size of the materials were computed to be in the range of 29-48 nm.

SEM and TEM studies

The SEM and TEM images of the samples are shown in Figure 3. The SEM and TEM micrographs (Figure 3a,b) of the V_2O_5 show a rodlike shape. Similar rodlike morphology has been reported by other researchers [15, 39]. The TEM image of the V_2O_5 /Ch-g-SA nanocomposite (Figure 3c) showed that the V_2O_5 was impregnated in the graft copolymer because the nano rods can be seen in the graft copolymer.

Equilibrium adsorption studies

Impact of contact time

The trend observed for the contact time was identical for both Q_e and R.E (Figure 4). There was a gradual increase in R.E and Q_e within the first 70 minutes. The increase could be attributed to the availability of unoccupied adsorption sites within the first 80 minutes, after which the V_2O_5 /Ch-g-SA surface became saturated and a subsequently no significant adsorption was observed.

Impact of varying of V_2O_5 /Ch-g-SA dose

MV adsorption onto V_2O_5 /Ch-g-SA nanocomposite was investigated by varying the adsorbent dose (0.05, 0.1, 0.15, 0.2,

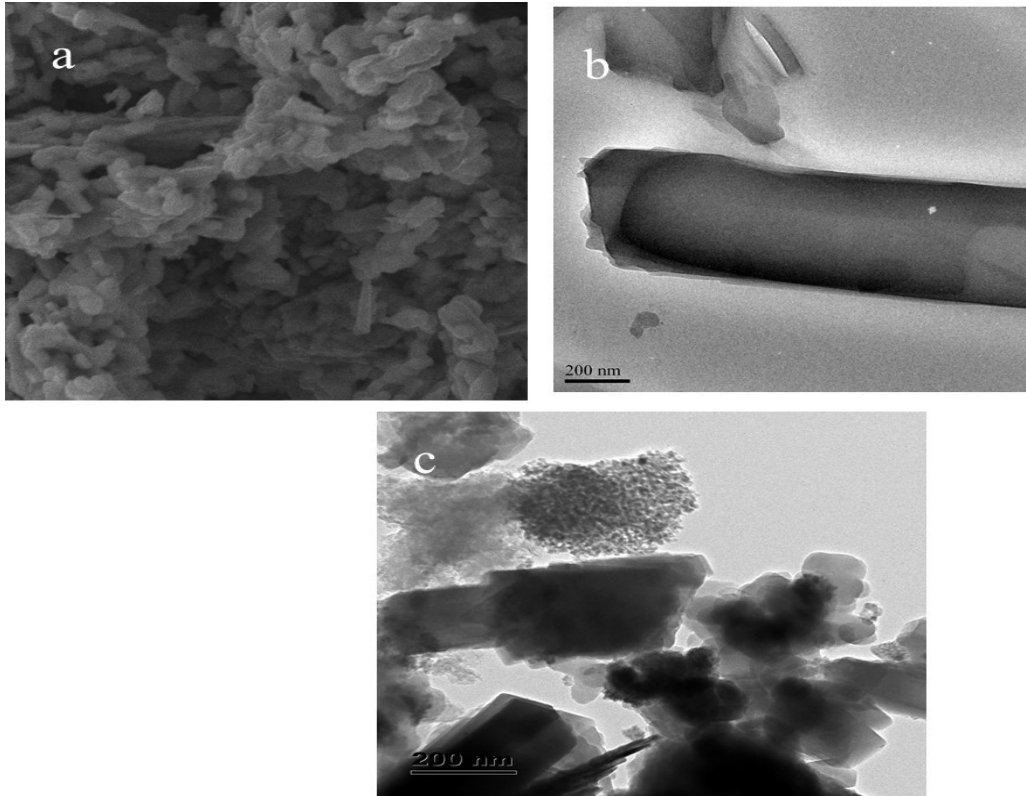


Figure 3: SEM of V₂O₅ nanoparticle (a). TEM of V₂O₅ nanoparticle (b) and TEM of V₂O₅/Ch- σ -SA nanocomposite (c).

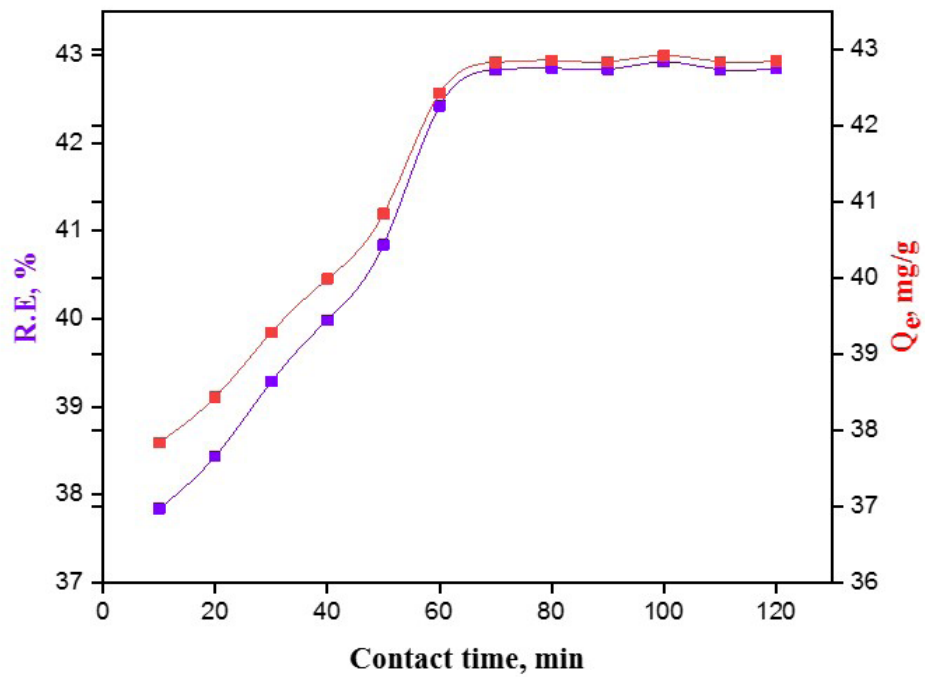


Figure 4: Impact of contact time on MV adsorption.

0.25, 0.3g/50 ml) in the dye solution while keeping other variables constant (Figure 5). An increase in removal efficiency was observed from 83.75% to 87.91% which may be attributed to the availability of vacant adsorption sites. However, the decrease observed from 85.16% to 81.31% could be as a result of aggregation of the adsorbent molecules leading to the observed decrease. Q_e declined from 83.75 mg/g to 11.62 mg/g with an addition in adsorbent dose. This may result from the overlapping of the $V_2O_5/Ch-g-SA$ surface area available to MV.

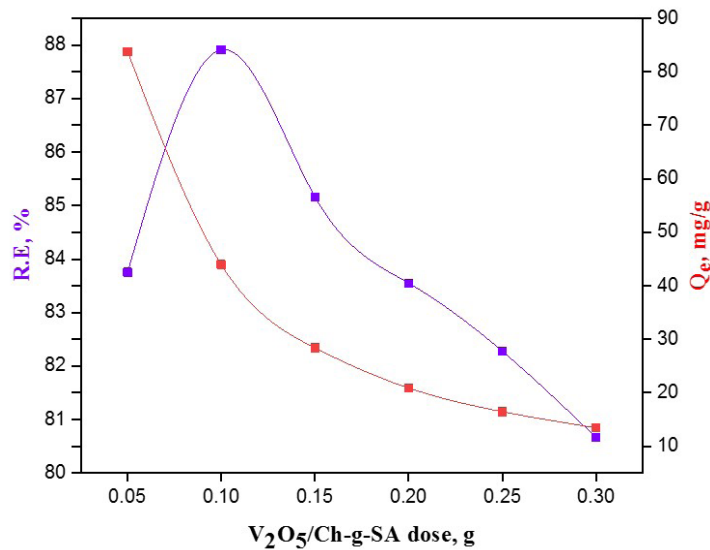


Figure 5: Effect of $V_2O_5/Ch-g-SA$ nanocomposite dose on MV adsorption.

Influence of initial concentration

From Figure 6, it can be seen that the removal efficiency, R.E and quantity of dye removed per unit mass, Q_e both increased. The increase in R.E may be attributed to vacant available adsorption sites as the concentration increased. The increase in Q_e may result from the significant mass transfer driving force towards the $V_2O_5/Ch-g-SA$ surface as concentration increased.

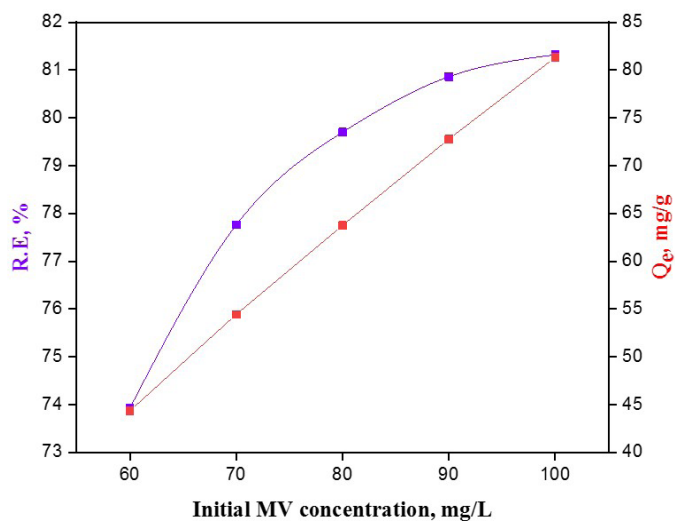


Figure 6: Effect of initial MV concentration on MV adsorption.

Effect of temperature

Figure 7 describes the effect of temperature on adsorption of MV onto $V_2O_5/Ch-g-SA$ nanocomposite at different temperatures of the MV test solution. With increasing temperatures, both R.E and Q_e increased from 83.30% to 86.32% and 83.30 mg/g to 86.32 mg/g respectively. This may be ascribed to the dye molecules acquiring adequate kinetic energy as temperature increases, allowing the adsorbate to adhere to the surface of the nanocomposite. In addition, the observed data could be indicative of an endothermic process.

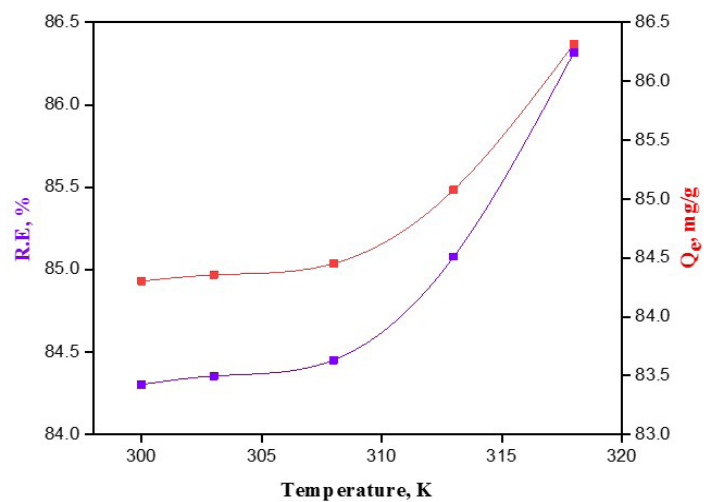


Figure 7: Effect of temperature on MV adsorption.

Effect of pH

The effect of pH on the removal of MV onto $V_2O_5/Ch-g-SA$ is presented in Figure 8. The adsorption capacity was low at pH 2. This could be due to the protonation of the amino groups in chitosan in acidic pH [40]. As the pH of the solution increases, interactions between carboxylic and amino groups of the nanocomposite allow for MV uptake. Similar findings have been reported [1,40].

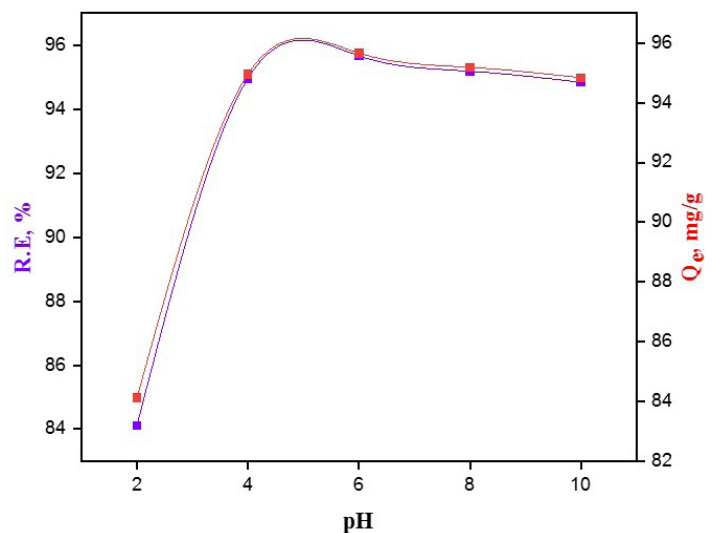


Figure 8: Effect of pH on MV adsorption.

Adsorption Isotherms

Adsorption isotherms are used to analyse the adsorbate-adsorbent interaction in the adsorption process. The data obtained from these models help to design appropriate adsorption systems. For this study, the adsorption data was fitted to the Langmuir, Freundlich and Dubinin-Radushkevich (D-R) isotherm models (Figure 9a-c). The Langmuir isotherm best suited the adsorption process ($R^2=0.9999$) compared to the Freundlich ($R^2=0.9958$) and Dubinin-Radushkevich ($R^2=0.9208$) isotherms. The monolayer adsorption capacity of $V_2O_5/Ch-g-SA$ was computed to be 77.52 mg/g and the value of the separation factor R_L was 0.00975 indicating a favourable adsorption because the value lies between zero and unity. The mean free energy E was computed to be 312.5 kJ/mol.

Adsorption Kinetics

The correlation coefficients R^2 of the pseudo-second order (0.9995) was observed to be larger than the pseudo-first order kinetic (0.8528) (Figure 10a,b). This means that the model was applicable over the entire period of adsorption. Similar findings have been reported [1,41].

Adsorption Thermodynamics

The values of ΔG° , ΔS° and ΔH° which are the thermodynamic

properties that describe the adsorption process are presented in Table 1. The negative values of ΔG° within the range of temperatures suggest the spontaneity and thermodynamically feasibility of the adsorption process. The positive value of ΔH° confirmed the endothermic nature of the process. The value of ΔS° indicated an affinity of MV species towards the $V_2O_5/Ch-g-SA$ surface and a decrease in disorderliness during the adsorption [42].

Table 1: Thermodynamic parameters of MV adsorption onto $V_2O_5/Ch-g-SA$ nanocomposite

ΔH° (kJ/mol)	ΔS° (kJ/mol)	ΔG° (kJ/mol.K)	300 K	303 K	308 K	313 K	328 K
6.62	0.035	-4.19	-4.24	-4.33	-4.53	-4.87	

Antimicrobial Activity

Microorganisms such as *Escherichia coli*, *Bacillus megaterium*, *staphylococcus aureus* and *Vibrio cholera* are known to cause water borne diseases. These microorganisms cause typhoid fever, diarrhea, dysentery, gastroenteritis and cholera. In this work, V_2O_5 nanoparticle and $V_2O_5/Ch-g-SA$ nanocomposite were investigated and tested on *Escherichia coli*, *Bacillus megaterium* and *staphylococcus aureus* which are Gram-positive and Gram-negative bacteria. The results (Figure 11) indicated that all the

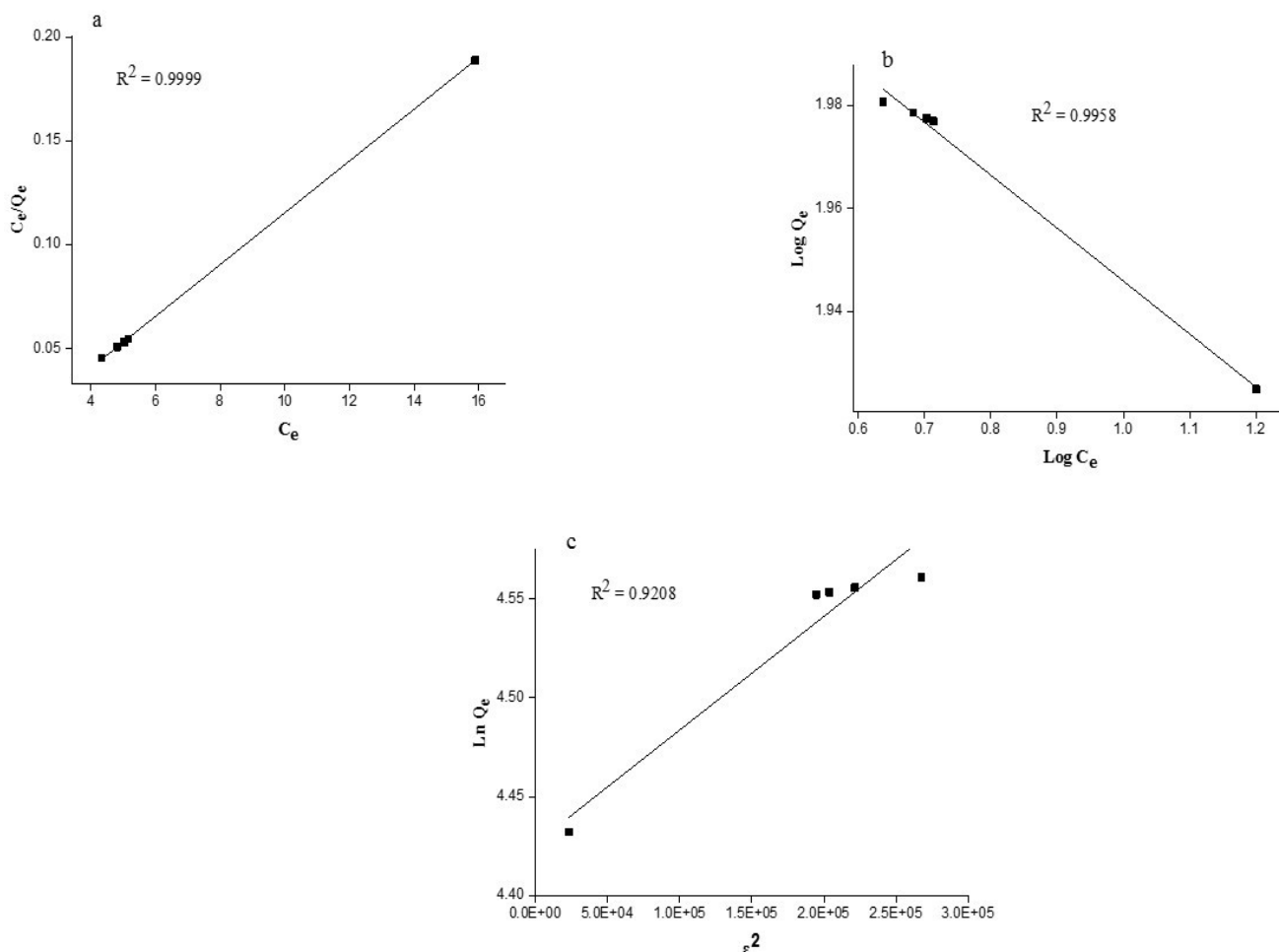


Figure 9: Langmuir (a), Freundlich (b) and Dubinin-Radushkevich (c) isotherm plots of MV adsorption onto $V_2O_5/Ch-g-SA$ nanocomposite.

samples had antimicrobial activity against these Gram positive and Gram-negative bacteria with more inhibition against *Staphylococcus aureus*. In all the microbes tested, V_2O_5 showed higher inhibition zones as compared to $V_2O_5/Ch-g-SA$ [21].

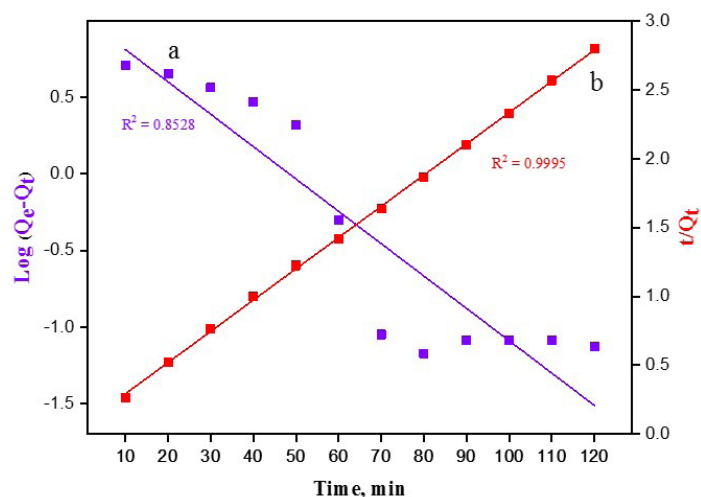


Figure 10: Pseudo-first order (a) and pseudo-second order (b) kinetic plots of MV adsorption onto $V_2O_5/Ch-g-SA$ nanocomposite.

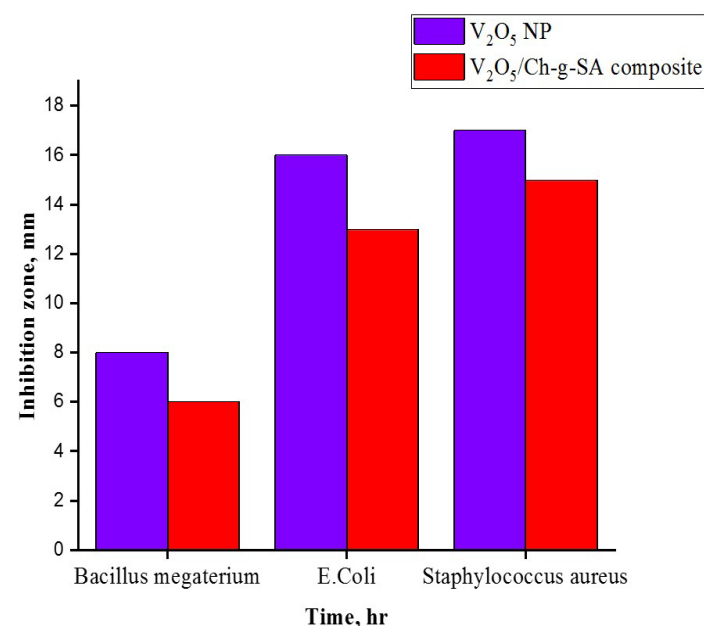


Figure 11: A 24-hour Inhibition zone on selected microbes.

Conclusion

V_2O_5 NP and $V_2O_5/Ch-g-SA$ nanocomposite was synthesized successfully. The study revealed that the material could be employed as an adsorbent for methyl violet (MV) dye uptake from wastewater. The FTIR spectra established the formation of V_2O_5 and its encapsulation into chitosan-graft-sodium alginate matrix. SEM and TEM confirmed the morphology of V_2O_5 to be a nanorod. The XRD pattern of V_2O_5 matched the crystalline orthorhombic phase of V_2O_5 . Batch adsorption tests indicated that the adsorption of MV

onto $V_2O_5/Ch-g-SA$ nanocomposite was dependent on adsorption kinetics such as pH, adsorbent dosage, temperature, contact time, initial dye concentration and temperature. The optimum MV removal dose was 0.1 g. The optimum pH and contact time for the effective removal of MV dye in water was in the weak acidic range (pH 6) and 80 minutes respectively. The Langmuir isotherm model and the pseudo-second order model best suited the adsorption data. The thermodynamic parameters inferred that the adsorption of MV onto V_2O_5 -copolymer was a spontaneous and thermodynamically feasible process. Antimicrobial studies showed that the material has an activity against Gram positive and Gram-negative bacteria with more inhibition towards *Staphylococcus aureus*.

Acknowledgement

We thank the Royal Society- Department for International Development (DFID) Africa Capacity Building Initiative (ACBI), UK, for their support towards this work. We also acknowledge the technical support from DST-CSIR National Center for Nanostructured Materials, CSIR in the characterization of the materials.

Funding

This work was partly funded by [43].

Data accessibility

The data collected in this research article is from the experiment. The information used to support the results of this study is included in the article and can also be accessed upon request from the corresponding author.

References

- Gokila S, Gomathi T, Sudha PN, et al. Removal of the heavy metal ion chromium(VI) using Chitosan and Alginate nanocomposites. *International Journal of Biological Macromolecules*. 2015; 104: 1459-1468.
- Singh KP, Mohan D, Singh VK, et al. Studies on distribution and fractionation of heavy metals in Gomti river sediments - A tributary of the Ganges. *India Journal of Hydrology*. 2005; 312: 14-27.
- Şen S, Demirel GN. Anaerobic treatment of real textile wastewater with a fluidized bed reactor. *Water Research*. 2003; 37: 1868-1878.
- Ben Mansour H, Houas I, Montassar F, et al. Alteration of in vitro and acute in vivo toxicity of textile dyeing wastewater after chemical and biological remediation. *Environmental Science and Pollution Research*. 2012; 19: 2634-2643.
- Chequer FMD, de Oliveira GAR, Ferraz ERA, et al. Textile dyes: dyeing process and environmental impact. *Intech*. 2013; 10: 5772-53659.
- Dos-Santos A, Bisschops IA, Cervantes F, et al. Effect of different redox mediators during thermophilic azo dye reduction by anaerobic granular sludge and comparative study between mesophilic (30 C) and thermophilic (55 C) treatments for decolourisation of textile wastewaters. *Chemosphere*. 2004; 55: 1149-1157.

7. Wijetunga S, Li XF, Jian CZ. Effect of organic load on decolourization of textile wastewater containing acid dyes in upflow anaerobic sludge blanket reactor. *Journal of Hazardous Materials*. 2010; 177: 792-798.
8. Przystas W, Zablocka-Godlewska E, Grabinska-Sota E. Biological removal of azo and triphenylmethane dyes and toxicity of process by-products. *Water, Air, and Soil Pollution*. 2012; 223: 1581-1592.
9. Hubbe MA, Hasan SH, Ducoste JJ. Cellulosic substrates for removal of pollutants from aqueous systems: A review. 1. Metals. *BioResources*. 2011; 6: 2161-2287.
10. Hassaan MA, Nembr AEL. Health and Environmental Impacts of Dyes: Mini Review. *Am Journal of Environmental Science and Engineering*. 2017; 1: 64-67.
11. Igberase E, Osifo P. Equilibrium, kinetic, thermodynamic and desorption studies of cadmium and lead by polyaniline grafted cross-linked chitosan beads from aqueous solution. *Journal of Industrial and Engineering Chemistry*. 2015; 26: 340-347.
12. Zhou YT, Nie HL, Branford-White C, et al. Removal of Cu²⁺ from aqueous solution by chitosan-coated magnetic nanoparticles modified with α -ketoglutaric acid. *Journal of Colloid and Interface Science*. 2009; 330: 29-37.
13. Mittal H, Ray SS. A study on the adsorption of methylene blue onto gum ghatti/TiO₂nanoparticles-based hydrogel nanocomposite. *International Journal of Biological Macromolecules*. 2016; 88: 66-80.
14. Xu P, Ming Zeng G, Lian Huang D, et al. Use of iron oxide nanomaterials in wastewater treatment: A review. *Science of the Total Environment*. 2012; 424: 1-10.
15. Dhayal Raj A, Pazhanivel T, Suresh Kumar P, et al. Self assembled V₂O₅ nanorods for gas sensors. *Current Applied Physics*. 2010; 10: 531-537.
16. Lala NL, Jose R, Yusoff MM, et al. Continuous tubular nanofibers of vanadium pentoxide by electrospinning for energy storage devices. *Journal of Nanoparticle Research*. 2012; 14: 1-9.
17. Im JS, Kwon O, Kim YH, et al. The effect of embedded vanadium catalyst on activated electrospun CFs for hydrogen storage. *Microporous Mesoporous Materials*. 2008; 115: 514-521.
18. Avansi W, De Mendonça VR, Lopes OF, et al. Vanadium pentoxide 1-D nanostructures applied to dye removal from aqueous systems by coupling adsorption and visible-light photodegradation. *RSC Advances*. 2015; 5: 12000-12006.
19. Carneiro-da-Cunha MG, Cerqueira M, Souza BWS, et al. Physical and thermal properties of a chitosan/alginate nanolayered PET film. *Carbohydrates Polymers*. 2010; 82: 153-159.
20. Fabryanty R, Valencia C, Soetaredjo FE, et al. Removal of crystal violet dye by adsorption using bentonite - alginate composite. *Journal of Environmental Chemical Engineering*. 2017; 5: 5677-5687.
21. Sharma S, Sanpui P, Chattopadhyay A, et al. Fabrication of antibacterial silver nanoparticle-Sodium alginate-chitosan composite films. *RSC Advances*. 2012; 2: 5837-5843.
22. Gupta D, Singh D, Kothiyal NC, et al. Synthesis of chitosan-g-poly(acrylamide)/ZnS nanocomposite for controlled drug delivery and antimicrobial activity. *International Journal of Biological Macromolecules*. 2015; 74: 547-557.
23. Pathania D, Gupta D, Al-Muhtaseb AH, et al. Photocatalytic degradation of highly toxic dyes using chitosan-g-poly(acrylamide)/ZnS in presence of solar irradiation. *Journal of Photochemistry and Photobiology A: Chemistry*. 2016; 329: 61-68.
24. Vijayalakshmi K, Devi BM, Latha S, et al. Batch adsorption and desorption studies on the removal of lead (II) from aqueous solution using nanochitosan/sodium alginate/microcrystalline cellulose beads. *International Journal of Biological Macromolecules*. 2017; 104: 1483-1494.
25. Ablouh EH, Hanani Z, Eladlani N, et al. Chitosan microspheres/sodium alginate hybrid beads: An efficient green adsorbent for heavy metals removal from aqueous solutions. *Sustainable Environment Research*. 2019; 29: 1-11.
26. Wu T, Huang J, Jiang Y, et al. Formation of hydrogels based on chitosan/alginate for the delivery of lysozyme and their antibacterial activity. *Food Chemistry*. 2018; 240: 361-369.
27. Langmuir I. The constitution and fundamental properties of solids and liquids. Part II.-Liquids. *Journal of the American Chemical Society*. 1917; 39: 1848-1906.
28. Dada AO, Olalekan AP, Olatunya AM, et al. Langmuir, Freundlich, Temkin and Dubinin-Radushkevich Isotherms studies of equilibrium sorption of Zn²⁺ onto phosphoric acid modified rice husk. *IOSR Journal of Applied Chemistry*. 2012; 3: 38-45.
29. Oyelude EO, Awudza JAM, Twumasi SK. Removal of acid blue 40 from aqueous solution by teak Leaf litter powder: Kinetics, thermodynamics and equilibrium study. *Journal of Materials and Environmental Science*. 2018; 9: 2087-2097.
30. Ho YS, McKay G. Pseudo-second order model for sorption processes. *Process Biochemistry*. 1999; 34: 451-465.
31. Molli M, Salian GD, Aditha SK, et al. Vanadium pentoxide nanoparticles based saturable absorbers. *America Institute of Physics Conference Proceedings*. 2012; 1461: 233-236.
32. Zhang Y, Zheng J, Wang Q, et al. One-step hydrothermal preparation of (NH₄)₂V₂O₈/carbon composites and conversion to porous V₂O₅ nanoparticles as supercapacitor electrode with excellent pseudocapacitive capability. *Applied Surface Science*. 2017; 423: 728-742.
33. Lawrie G, Keen I, Drew B, et al. Interactions between alginate and chitosan biopolymers characterized using FTIR and XPS. *Biomacromolecules*. 2007; 8: 2533-2541.
34. Viswanathamurthi P, Bhattarai N, Kim HY, et al. Vanadium

-
- pentoxide nanofibers by electrospinning. *Scripta Materialia*. 2003; 49: 577-581.
35. Partlow DP, Gurkovich SR, Radford KC, et al. Switchable vanadium oxide films by a sol-gel process. *Journal of Applied Physics*. 1991; 70: 443-452.
36. Yoksan R, Chirachanchai S. Silver nanoparticle-loaded chitosan-starch based films: Fabrication and evaluation of tensile, barrier and antimicrobial properties. *Materials Science and Engineering*. 2010; 30: 891-897.
37. Li X, Xie H, Lin J, et al. Characterization and biodegradation of chitosan-alginate polyelectrolyte complexes. *Polymer and Degradation Stability*. 2009; 94: 1-6.
38. Chen Z, Mo X, He C, et al. Intermolecular interactions in electrospun collagen-chitosan complex nanofibers. *Carbohydrates Polymer*. 2008; 72: 410-418.
39. Asim N, Radiman S, Yarmo MA, et al. Vanadium pentoxide: Synthesis and characterization of nanorod and nanoparticle V₂O₅ using CTAB micelle solution. *Microporous Mesoporous Materials*. 2009; 120: 397-401.
40. Abou El Fadl FI. Radiation grafting of ionically crosslinked alginate/chitosan beads with acrylic acid for lead sorption. *Journal of Radioanalytical and Nuclear Chemistry*. 2014; 301: 529-535.
41. Maity J, Ray SK. Enhanced adsorption of methyl violet and congo red by using semi and full IPN of polymethacrylic acid and chitosan. *Carbohydrate Polymer*. 2014; 104: 8-16.
42. Saha P, Chowdhury S. Insight Into Adsorption Thermodynamics. *Thermodynamics*. 2011.